ISSN 1330-3651 (Print), ISSN 1848-6339 (Online)
https://doi.org/10.17559/TV-20241108002115
Original scientific paper

Study of the Effects of Wind Turbines Integration Into the Electricity Grid

Laila BOUAZIZ, Mehdi DHAOUI, Mouna BEN HAMED, Aymen FLAH, Habib KRAIEM*, Mishari Metab ALMALKI, Ahmad A. MOUSA

Abstract: This work presents a comprehensive study of the effects of integrating wind turbines into the electrical grid, focusing on enhancing grid stability. This paper proposes a novel method to improve the stability of grid-connected fixed-speed wind turbines by employing static synchronization technology based on static reactive power compensation (STATCOM). The system operation with and without STATCOM and the transient voltage stability analysis of the wind turbine were thoroughly investigated and verified through detailed simulation studies conducted in the MATLAB/Simulink environment. Furthermore, the effectiveness of the STATCOM approach was evaluated under various fault conditions and operating scenarios. The comparison results clearly demonstrate the robustness and efficiency of the STATCOM-based approach, significantly enhancing the stability and performance of the network integrating wind turbines, thus ensuring reliable and efficient power generation.

Keywords: grid integration; reactive power compensation; statcom; voltage stability; wind farm

1 INTRODUCTION

The integration of wind turbines into the electrical grid impacts the stability, reliability, and efficiency of the energy system. As wind energy's role in the energy mix grows, it becomes essential for grid operators, policymakers, and engineers to address these effects. This paper discusses the challenges of wind turbine integration and suggests solutions for enhancing grid stability.

State of the Art: Wind energy is inherently intermittent, making it difficult to align energy supply with demand. High wind speeds may coincide with low energy demand and vice versa [1]. Such dynamics can cause voltage imbalances, power fluctuations, transmission losses, poor power factors, and potential shutdown of wind farms. To mitigate these issues, grid operators enforce grid codes specifying requirements at the Point of Common Coupling (PCC), including reactive power control, active power control, system fault tolerance, frequency response, and voltage fluctuation management [2].

Problem Statement: Wind farm developers utilize various strategies to meet grid codes and enhance turbine performance. Full-power converters in wind turbines improve compliance with grid standards. In systems with variable-speed synchronous generators, the wind generator mimics conventional generators and connects to the grid through static power converters [3]. However, WTGs require robust components to handle mechanical forces during grid events. Increased resynchronization frequency elevates mechanical failure risks. Additionally, greater distance between turbines and the collection system reduces compliance with grid regulations. Another approach is using reactive power compensation systems at the PCC. These systems manage reactive power automatically to improve voltage stability, injecting reactive power during low-voltage conditions and absorbing excess power during high-voltage conditions. This precision improves response speed and automated control [3].

Proposed Solution: The variable and intermittent nature of wind energy, influenced by weather conditions, challenges grid stability. Unlike conventional power plants, wind turbines have low inertia, making frequency stability maintenance challenging. Solutions include sophisticated control systems, turbine designs with synthetic inertia, and reactive power compensation technologies like Flexible AC Transmission Systems (FACTS) or voltage regulation features [2]. Integrating flexible generation sources such as gas turbines or hydropower and employing Demand-Side Management (DSM) can help align energy consumption with wind availability. Additionally, energy storage solutions like batteries and pumped hydro systems can store excess wind energy during high production and release it during low generation periods. However, large-scale energy storage systems remain financially challenging. Enhancing interconnections between regions can also reduce the impact of wind variability by distributing resources over broader geographical areas [3].

Paper Organization: Section 2 discusses reactive power compensation methods, including Capacitor Banks, Static Var Compensator (SVC), Static Synchronous Series Compensator (SSSC), and Static Synchronous Compensator (STATCOM). Section 3 covers grid architecture with integrated wind turbines and related challenges. Section 4 details the modeling of wind generator components like PMSG models, power converters, rectifiers, DC models, inverters, filters, and grids, including the PMSG-based wind turbine model. Section 5 presents the Pert-Unit System for simplifying electrical grid and system component analysis. Section 6 describes STATCOM control schemes, including constant reactive power control, voltage control, and constant reactive current control. Section 7 discusses the control signals produced by the STATCOM control system, focusing on optimal control methods. Section 8 provides simulation results, comparing scenarios with and without STATCOM, analyzing turbine response in normal and fault conditions. Finally, Section 9 offers conclusions and recommendations for enhancing grid stability and wind energy integration.

2 REACTIVE POWER COMPENSATION

To ensure that the wind farm complies with the requirements of the grid code, the installation of a reactive power compensator is necessary, either associated with an individual wind turbine or at the common coupling point (PCC) of a wind farm.

Most reactive power compensators utilized in various wind energy systems today are of the shunt type. These compensators consist of static power converters, switching control devices, and passive capacitive/inductive elements.

There are several devices employed to manage reactive power, with a specific focus in this study on the Static Synchronous Compensator (STATCOM). Other devices include capacitor banks, Static Var Compensators (SVC), and Static Synchronous Series Compensators (SSSC) [4, 16].

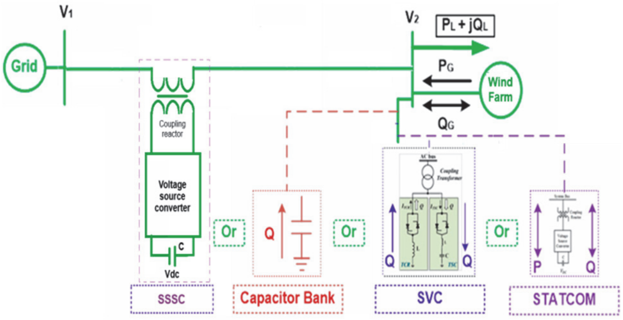

Figure 1 Schematic/connection diagram of capacitor bank, SVC, STATCOM and SSSC compensator in grid system

2.1 Capacitor Banks

Capacitor banks are extensively utilized for reactive power compensation due to their cost-effectiveness in operation. They enhance power factor, leading to improved voltage regulation. The schematic representation of the capacitor bank is illustrated in Fig. 1. Switched capacitor banks are primarily used in shunt configurations at the point of common coupling (PCC) of renewable energy systems to provide enhanced reactive power support [17, 18]. However, these systems can generate significant switching transients, high-frequency harmonics, and may lead to resonance problems. Furthermore, their dynamic response is not optimal, as the reactive power supplied is directly related to the square of the voltage. As a result, when the system voltage falls below the rated level, the reactive power supplied is less than what is required. Conversely, if the system voltage exceeds the nominal level, it can lead to overvoltage conditions [5].

2.2 Static Var Compensator (SVC)

SVC is a FACTS device utilized for reactive power management in wind farms, as illustrated in Fig. 1. It enhances the dynamic response to voltage fluctuations, resulting in improved voltage regulation and increased system stability by delivering rapid reactive power. The primary components of SVC include a thyristor-controlled reactor (TCR), a thyristor-switched capacitor (TSC), and a harmonic filter, as depicted in Fig. 1. Consequently, it functions in both capacitive and inductive modes [19, 20]. When the power system operates at a leading power factor, the reactor is engaged to absorb reactive power and reduce the system voltage. In contrast, when operating at a lagging power factor, the capacitor is activated to supply reactive power, thereby elevating the voltage. Nevertheless, SVC lacks an effective mechanism for damping transients [6, 21].

2.3 Static Synchronous Series Compensator (SSSC)

The connection and schematic diagram of the SSSC are illustrated in Fig. 1. The SSSC consists of a coupling transformer, a voltage source converter (VSC), and a DC capacitor. Structurally, the SSSC is similar to a STATCOM; however, it functions as a series compensation device, operating as both a series reactor and a series capacitor. Notably, it possesses the ability to inject voltage independently of the line current [22, 23]. By adjusting the X/R ratio of the network, it mitigates both reactive and resistive voltage drops. The SSSC injects voltage and regulates it through rapid control at the point of common coupling (PCC). By reducing effective reactance, the SSSC improves the power transfer capability of the power system. It can exchange both active power (P) and reactive power (Q) within the network, thereby enhancing voltage regulation and providing fault ride-through (FRT) through voltage injection [7, 24].

2.4 Static Synchronous Compensator (STATCOM)

STATCOM is a significant device within the Flexible AC Transmission Systems (FACTS) category, consisting of a coupling reactor, a voltage source converter (VSC), and a DC capacitor, as illustrated in Fig. 1. This device enhances power factor (PF) and voltage regulation at the point of common coupling (PCC), thereby increasing the power transmission capacity and overall system stability [25, 26]. It is capable of supplying and absorbing reactive power according to the demands of the system by functioning in either capacitive or inductive modes. In scenarios where the power system experiences a capacitive load and operates at a leading power factor, STATCOM assumes an inductive role by absorbing reactive volt-amperes (*Vars*). Conversely, when the power system operates at a lagging power factor, it adopts a capacitive role by supplying Vars to stabilize the voltage and meet reactive power requirements. Additionally, STATCOM is utilized in conjunction with a harmonic filter to achieve improved power quality (PQ). It effectively restores PCC voltage by providing a rapid dynamic response to voltage fluctuations and enhances the transient stability of the power system [5, 27].

3 GRID ARCHITECTURE WITH INTEGRATION OF A WIND TURBINE

The diagram presented in Fig. 2 shows the architecture of the network with the integration of a wind turbine. The system includes a conventional generator, a wind farm and a power load. A static synchronizer type STATCOM establishes the stabilization of the electrical network.

A wind farm consisting of six 1.5 MW wind turbines is connected to a 25 kV distribution system and exports power to a 120 kV grid through a 25 km 25 kV feeder.

The 9 MW wind farm is simulated by three pairs of 1.5 MW wind-turbines. Wind turbines use permanent magnet synchronous generators (PMSG) [28].

The stator winding is directly connected to the 50 Hz grid, and the rotor is driven by a variable-pitch wind turbine. The pitch angle is adjusted to limit the generator's output power to its nominal value in the event that winds exceed the nominal speed (9 m/s). To produce power, the PMSG speed needs to be slightly higher than the synchronous speed. At no load, the speed ranges roughly between 1 pu and 1.005 pu. Every wind turbine has a protective system that keeps an eye on the machine's speed, voltage, and current [29, 30].

The reactive power absorbed by the PMSG is partially compensated by capacitor banks connected to each wind turbine's low voltage bus (400 kva for each pair of 1.5 MW turbine). To maintain the 25 kV voltage at bus B25 close to 1 pu, we use a 3 MVar STATCOM with a 3% droop setting to provide the remaining reactive power.

The turbine mechanical power is measured by turbine speed for wind speeds that range from 4 m/s to 10 m/s. The nominal mechanical power (1 pu = 3 MW) is generated by the wind speed of 9 m/s.

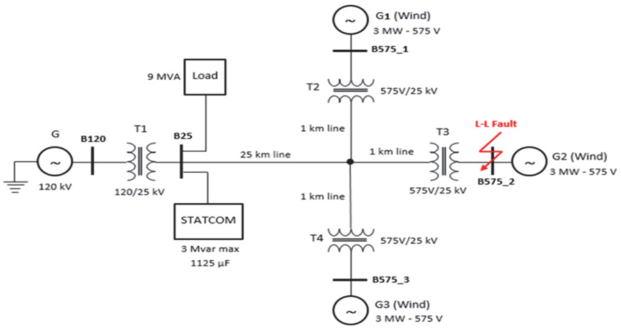

Figure 2 Grid Architecture with integration of a wind farm turbine

To test the stability of the grid system with and without STATCOM, a line-line fault (short circuit) was created in the system from 15 s to 15.1 s. The device STATCOM will be used to address the stability issue caused by this disturbance-type flaw in the system.

4 MODELING THE COMPONENTS OF THE WIND GENERATOR

The generator choice depends on factors like cost, efficiency, maintenance, and installation location (onshore/offshore). PMSG offers high efficiency for offshore use but is costly. DFIG is popular for onshore farms due to affordability and good control. SCIG is robust and simple but unsuitable for modern variable-speed turbines. SG provides an alternative to PMSG but requires higher maintenance.

4.1 PMSG-Based Wind Turbine Model

A wind farm consisting of six 1.5 MW wind turbines. The wind generator considered in this work has a power of 1.5 MW with a blade radius of 48 m. The wind turbine works at a variable speed for a nominal wind of 9 m/s. The mechanical power is provided by Eq. (1) [5, 31]:

$$P_t = \frac{1}{2} \cdot \rho \cdot S \cdot C_p(\lambda, \beta) \cdot V^3 \tag{1}$$

where ρ is the air density approximately equal to 1.223 kg/ m^3, S is the swept area by the wind turbine blades and V is the wind speed. λ and β are respectively the specific speed and the pitch angle of the blades [6].

C_p is the power coefficient of the wind turbine, whose Bitz limit is 0.59 [7], expressed by Eq. (2).

$$C_P(\lambda, \beta) = 0.52\left(151/\lambda_i - 0.58\beta - 0.002 \cdot \beta^{2.14} - 10.2\right) \cdot \\ \cdot \exp^{-18.4/\lambda_i} \tag{2}$$

Where:

$$\lambda_i = \frac{1}{\lambda + 0.02\beta} - \frac{0.003}{\beta^3 + 1} \tag{3}$$

Fig. 3 provide the characteristics of the C_p coefficient.

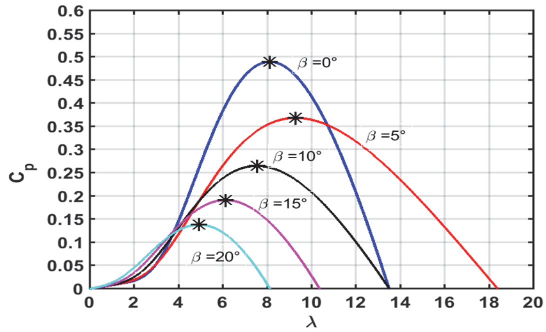

Figure 3 Characteristics of the power coefficient C_p (λ, β).

By utilizing relation Eq. (1), we can derive the characteristics of the turbine's mechanical power for various wind speeds. These characteristics pertain to a turbine with a radius of 48 meters.

4.2 PMSG Model

The wind system being studied uses a synchronous machine with permanent magnets. Eq. (4) provide the machine model in the Park frame of reference [8]:

- $V_{sd,q}$: the direct and quadrature components of the stator voltages.
- $i_{sd,q}$: the direct and quadrature components of the stator currents.
- $\phi_{sd,q}$ and ϕ_r : the direct and quadrature components of the stator fluxes and the flux of the permanent magnets.
- $L_{d,q}$: the direct and quadrature inductances of the stator coils.
- θ_r: the electrical angle defined by the position of the phase axis (a) of the stator by contribution to the axis of the rotor magnet (d).

$$\begin{aligned} v_{sd} &= R_s \cdot i_{sd} + L_d \frac{\mathrm{d}i_{sd}}{\mathrm{d}t} - \omega_r L_q i_{sq} \\ v_{sq} &= R_s \cdot i_{sq} + L_d \frac{\mathrm{d}i_{sq}}{\mathrm{d}t} + \omega_r L_d i_{sq} + \omega_r \phi_r \end{aligned} \tag{4}$$

The reference frame (d, q) linked to the rotor rotates with a speed expressed by Eq. (5).

$$\omega_r = \frac{\mathrm{d}\theta_r}{\mathrm{d}t} = p \cdot \Omega_r \tag{5}$$

Such that p is the number of pole pairs and Ω_r is the mechanical speed of the GSAP rotor.

4.3 Modelling of Power Converters

The general structure shown in Fig. 4 is used for the integration of wind turbines based on a GSAP into the electrical grid. Power converters are necessary to transfer energy from the wind generator to the grid.

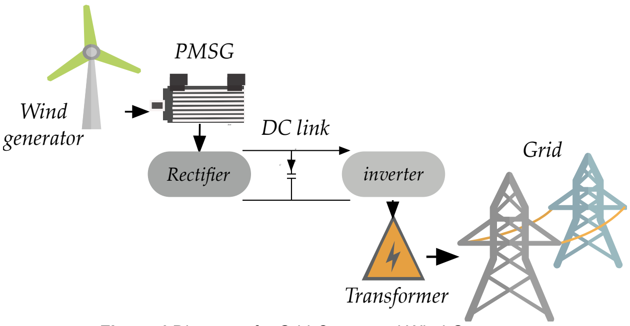

Figure 4 Diagram of a Grid-Connected Wind Generator

4.4 Rectifier Model

The input voltages for the rectifier are defined based on the voltage supplied by the GSAP generator and the DC bus voltage by Eq. (6).

$$\begin{aligned} U_{ab} &= (k_a - k_b) \cdot V_{dc} \\ U_{bc} &= (k_b - k_c) \cdot V_{dc} \\ U_{ca} &= (k_c - k_a) \cdot V_{dc} \end{aligned} \quad (6)$$

With k_i the state of the control signals of the switches of arms i, where: $i = a, b, c$.

$k_i = 0$: open state of the switch and $k_i = 1$: closed state of the switch. The rectifier's DC bus current output is expressed by Eq. (7):

$$i_{rec} = k_a \cdot i_a + k_b \cdot i_b + k_c \cdot i_c \quad (7)$$

4.5 DC Model

To establish the mathematical model of the DC bus, we need to calculate the voltage across the capacitor. i_{rec} is the input current and i_{inv} is the output current. V_{dc} is the voltage insisde the capacitor. The two currents (the rectifier's and the inverters) that are modulated by the two converters circulate at the node where the capacitor's current originates.

$$v_{dc} = \frac{1}{C}\int (i_{rec} - i_{inv}) \cdot \mathrm{d}t \quad (8)$$

4.6 Modelling of Inverter

The voltage inverter is essential for grid interfacing systems. It allows, among other things, to control the active and reactive powers exchanged with the network. It can be used in inverter mode or in rectifier mode but the modeling remains the same in both cases [10].

For two main reasons, the converter used in our study is of a double parallel type, similar to that of the rectifier, and consists of IGBTs and antiparallel diodes controlled by pulse width modulation (PWM):

- Modify the harmonic content of the output voltage to push its harmonics towards higher ranks and consequently, frequencies. This will facilitate the filtering of the voltage and make it easier to adjust.
- Permit adjustment of the effective value of the voltage's fundamental, which is crucial when dealing with machines that are network-connected.
- The inverter consists of three arms and two switches for each arm, (K_1, K_2), (K_3, K_4), (K_5, K_6), which are controlled in a complementary manner in order to avoid the short circuit.
- The law of meshes gives Eq. (9):

$$\begin{aligned} V_a &= \frac{1}{3}(2k_a - k_b - k_c) \cdot V_{dc} \\ V_b &= \frac{1}{3}(2k_b - k_a - k_c) \cdot V_{dc} \\ V_c &= \frac{1}{3}(2k_c - k_b - k_a) \cdot V_{dc} \end{aligned} \quad (9)$$

4.7 Modelling of Filter

At the output of the inverter, the currents are never sinusoidal. They have harmonics. To reduce these harmonics of the currents injected into the network, a filter is added to the output of the inverter. The latter is of type (LCL) and plays the role of a current source in relation to the network. In order to evaluate the performance of the network-side conversion using the LCL filter, we utilize the phase diagram in Fig. 5.

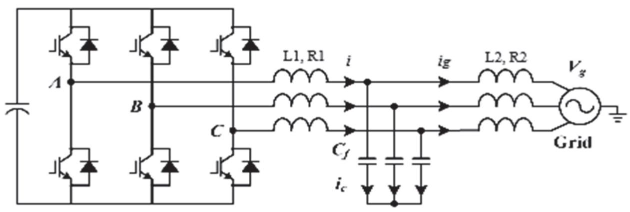

Figure 5 LCL filter connected to the output of the grid-connected inverter

According to the model in Fig. 6, the LCL filter equations referred to in the line are:

$$\begin{aligned} v_c &= v_a - R_1 \cdot i - L_1 \frac{\mathrm{d}i}{\mathrm{d}t} \\ v_g &= v_c - R_2 \cdot i_g - L_2 \frac{\mathrm{d}i_g}{\mathrm{d}t} \\ v_c &= \frac{1}{C_f}\int i_c \mathrm{d}t \end{aligned} \quad (10)$$

The transfer function between the grid current (i_{ag}) and the inverter voltage (V_a) (line a), ignoring the impact of resistances, can be represented by the Eq. (10).

$$H_F(p)=\frac{i_{ga}}{V_a}=\frac{1}{C_f L_1 L_2 p^3+p(L_1+L_2)}= \\ =\frac{Z_F^2}{p(p^2+\omega_{res}^2)} \tag{11}$$

With: $Z_F=\frac{1}{\sqrt{L_1 L_2 C_f}}$ is the filter impedance.

According to Eq. (11), the resonance frequency of the LCL filter is determined by Eq. (12).

$$\omega_{res}=2\pi f_{res}=\sqrt{\frac{L_1+L_2}{L_1 L_2 C_f}} \tag{12}$$

4.8 Modelling of Grid

The electrical grid model includes a line inductance L_2 and a resistance R_2 that are linked to the inverter via the LCL filter.

The electrical network in the Park reference frame of pulsation ωg is represented by the Eq. (13).

$$v_d=L_2\frac{\mathrm{d}i_{gd}}{\mathrm{d}t}+R_2\cdot i_{gd}-\omega_g L_2 i_{gq}+v_{gd} \\ v_d=L_2\frac{\mathrm{d}i_{gq}}{\mathrm{d}t}+R_2\cdot i_{gq}-\omega_g L_2 i_{gd}+v_{gq} \tag{13}$$

With: $v_{d,q}$: Single voltages output from the inverter, $v_{dq,g}$: Single voltages of the electrical grid, $i_{dq,g}$: Currents supplied to the electrical grid, the active and reactive powers supplied to the network are determined by the relationships Eq. (14).

$$P_g=\frac{3}{2}\left(v_{gd}\cdot i_{gd}-v_{gq}\cdot i_{gq}\right) \\ Q_g=\frac{3}{2}\left(v_{gq}\cdot i_{gd}-v_{gd}\cdot i_{gq}\right) \tag{14}$$

5 PERT-UNIT SYSTEM

The Per-Unit (p.u.) system is a method used in power system analysis to normalize system quantities like voltage, current, impedance, and power. This approach simplifies calculations, particularly when dealing with transformers, generators, and various parts of a power system that operate at different voltage levels [10].

The (p.u.) system expresses electrical quantities as a fraction of a defined base value, making it easier to compare and analyze different components within the power system. Instead of using actual units (volts, amperes, ohms, etc.), the per-unit system uses relative values.

To use the per-unit system, you first need to define base values for the quantities of interest. Commonly, base values for voltage (V_B), power (S_B), and sometimes impedance (Z_B) and current (I_B) are chosen.

With:

- Base Power (S_B): Typically expressed in MVA (megavolt-amperes).
- Base Voltage (V_B): Typically expressed in kV (kilovolts).
- Base Impedance (Z_B): Calculated using:

$$Z_B=\frac{U_B^2}{S_B} \tag{15}$$

For three-phase systems, the base current is calculated as follows in Eq. (16). Power (S), voltages (U), and currents (I) are expressed in *tl* relative unit system (p.u) by Eq. (17) :x=[S, U, I]. B refers to base or nominal index.

$$I_B=\frac{S_B}{\sqrt{3}\cdot U_B} \tag{16}$$

$$x_{(p.u.)}=\frac{x}{x_B} \tag{17}$$

The proposed grid's fundamental data are:

$$S_B=10\ \mathrm{MVA},\ U_B=25\ \mathrm{kV} \\ I_B=231\ \mathrm{A},\ Z_B=62.5\ \Omega$$

6 CONTROL STRATEGIES OF A STATCOM

A Static Synchronous Compensator (STATCOM) is a type of Flexible AC Transmission System (FACTS) device used in power systems for reactive power compensation, voltage control, and improving power system stability. It achieves these goals by controlling the voltage at a connection point in a grid, effectively managing the flow of reactive power [4-12].

The control strategies for a STATCOM involve regulating its output to maintain desired system conditions, such as stable voltage levels or improved power quality.

6.1 Constant Reactive Power Control

When TSO has multiple sources of reactive power available and the objective is to select the most suitable one, a control technique that maintains a STATCOM's reactive power constant is typically used. Generally speaking, a STATCOM is not the most cost-effective source for a continuous reactive power supply because of its higher losses in comparison to passive components (such as reactors and condensers) [4-13].

6.2 Voltage Contro

The STATCOM's current in voltage control is determined by the voltage at its connecting point. The current is regulated so that it depends linearly on the voltage differential between the reference voltage, UREF, and the network voltage, U Network. Fig. 6 and Fig. 7 show the U/I control characteristic. The operating points at different reference voltages are indicated by dashed blue lines, while solid blue lines delineate the boundaries of the control region [4].

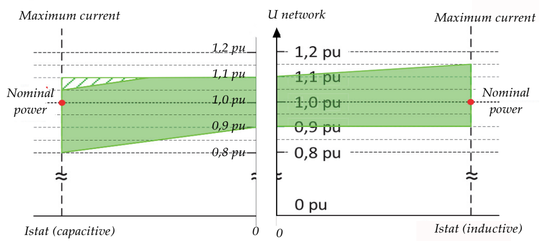

Figure 6 U/I operating characteristic of a STATCOM [11]

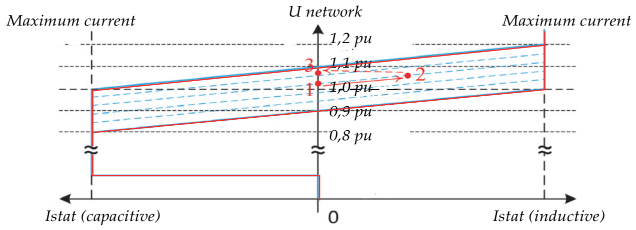

Figure 7 U/I operating characteristic of a STATCOM [11]

6.3 Constant Reactive Current Control

Typically, "constant reactive current" control is not used as a stand-alone control method. It is used more as a constraint on other control schemes to safeguard the STATCOM's power electronics, which are restricted by their maximum current [3, 4, 14].

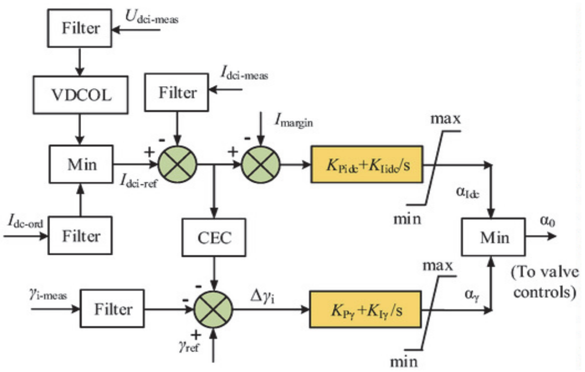

Figure 8 Diagram of STATCOM control

7 CONTROLLING SIGNAL GENERATING BY CONTROL SYSTEM STATCOM

The Fig. 8 shows the STATCOM control diagram. Controlling is nothing but one type of feedback system: V_{ABC} or I_{ABC}. Feedback signals are used for controlling. The use of control is based on the V_{abc} to V_{dqo} transformation theory, the V_{abc} to V_{dqo} and I_{abc} to I_{dq0} blocks are in phase loop locked by three-phase PLL blocks. The second order filter is a low-pass filter, V_{abc} and I_{abc} feedback signals are obtained from Bus_statcom. Two PI regulations are used in the control system, with different k_p and k_i gains. The choice of STATCOM depends on factors such as the scale of application, stability and robustness. The Parallel STATCOMs are better suited for large-scale applications where reliability, fast response, and scalability are required. On the other hand, STATCOM with Two PI Controllers are more appropriate for medium-scale applications with moderate compensation requirements. The following discreption summarizes the comparison between parallel STATCOMs and STATCOMs with Two PI controllers.

Parallel STATCOMs are ideal for large power systems and high dynamic fluctuations due to reliability and fast response. For industrial systems and low-cost reactive power support, STATCOMs with PI controllers offer simplicity and cost-effectiveness.

8 SIMULATION RESULTS AND DISCUSSIONS

The wind turbine model and the STATCOM model (from the FACTS library) are phasor models that allow for transient stability studies with long simulation times [4-15]. In this research, the system is simulated for 20 seconds. The "Wind 1" through "Wind 3" blocks regulate the wind speed applied to each turbine [15].

The wind speed for "Wind Turbine1" is first set to 8 m/s and then increased to 11 m/s from $t = 2$ s in 3 seconds.

The same wind gust is applied to turbines 2 and 3 with a delay of 2 and 4 seconds respectively.

8.1 Turbine Reaction in the Typical Scenario

Fig. 9 shows the active and reactive power, wind speed and angle of attack for each turbine under normal conditions. For each pair of turbines, the active power produced (with wind speed) starts to increase uniformly and reaches its nominal value of 3 MW in about 8 seconds. During this period, the turbine speed increases from 1.0028 pu to 1.0047 pu. Initially, the angle of attack of the turbine blades is zero degrees. When the output power exceeds 3 MW, the angle of attack is increased from 0 to 8 degrees to restore the output power to the rated value. Note that the consumed reactive power increases with the increase in active power produced. At rated power, each pair of wind turbines absorbs 1.47 Mvar.

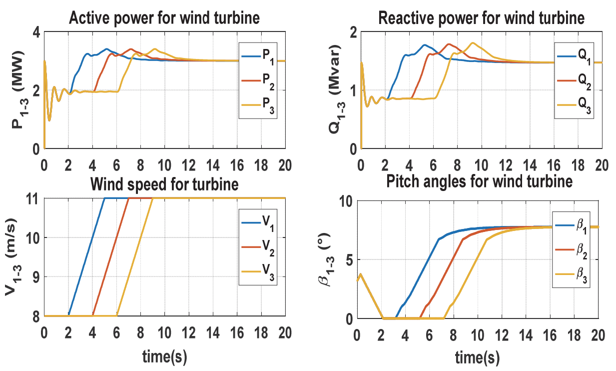

Figure 9 Turbine reactions in the typical scenario

The voltage, current, active power, and reactive power measured on the B25 bus are shown in Fig. 10. At a wind speed of 11 m/s, the total output power is 9 MW and the Statcom maintains the voltage at 0.984 Pu by generating 1.62 Mvar ("B25 bus" and "Statcom").

8.2 Turbine Reaction in Case of Fault

Then, a temporary fault is applied to the low voltage terminals (575V) of "Wind Turbine 2" from $t = 15$ s to 15.1 s.

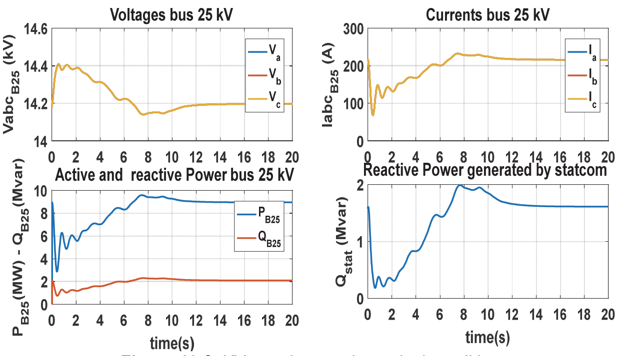

Figure 10 25KV reactions under typical conditions.

Fig. 11 and Fig. 12 show the response signals of each turbine and the characteristics measured on the 25 kV bus when the fault occurs, respectively.

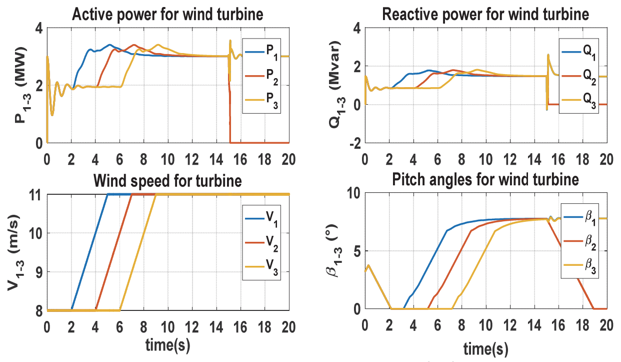

Figure 11 Turbine reactions in case of a fault

At $t = 15$ s, a line fault is applied to the connection of wind turbine 2, which triggers the turbine at $t = 15.11$ s. In the case of a fault (short circuit) between lines a and b during time 15 s to 15.1 s, the values measured on the wind bus (Fig. 13) show an unstable voltage level until Time 15.11 s, with an increase in current and a degradation of performance. Note that in the "Wind Turbine Protection" block, the trip is initiated by the AC under voltage protection. Therefore, after the tripping of turbine 2, turbines 1 and 3 continue to generate 3 MW each.

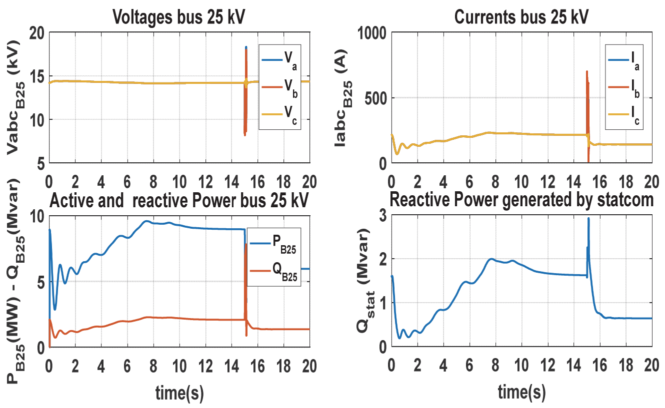

Figure 12 25 kV bus reactions in the faulty case with STATCOM

When the STATCOM compensator is connected (Fig. 13 and Fig. 14) and the fault is present, the voltage becomes more stable.

In fact, after the error is eliminated, the voltage remains unstable only until 15.11 s. In summary, we can see that the addition of the STATCOM compensator improves the stability of the transient voltage.

8.3 The Effect of STATCOM

In this case, we present the simulation results without "STATCOM". According to (Fig. 13 and Fig. 14), we observe that because of the lack of reactive power support, the voltage at bus "B25" now drops to 0.91 pu. This low voltage condition results in an overload of the PMSG of "Wind Turbine1"."Wind Turbine 1" is tripped at $t = 14.43$ s because in the "Wind Turbine Protections" block, the trip has been initiated by the AC overcurrent protection.

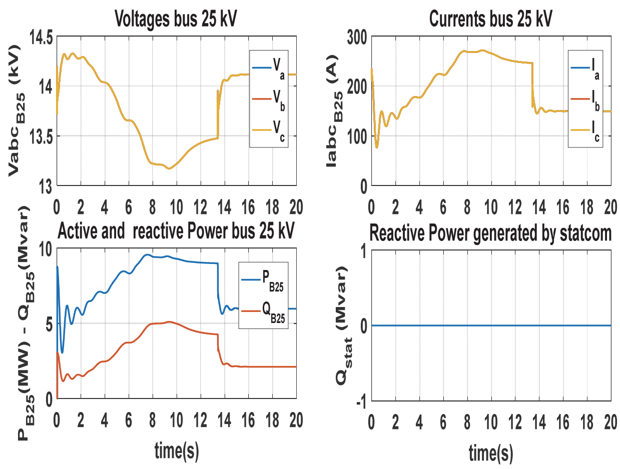

Figure 13 25 KV bus reactions without STATCOM

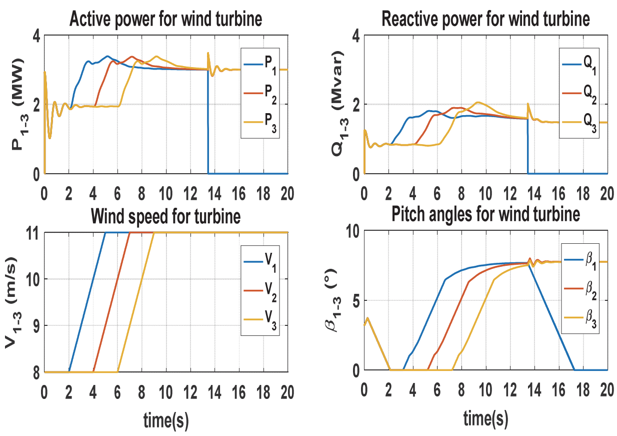

Figure 14 Turbine reactions without STATCOM

The comparison between the two cases, With and Without STATCOM, can be summarized in Tab. 1.

Table 1 Perfroamnces With and Withou STATCOM

Performance Criteria	Without STATCOM	With STATCOM
Voltage Stability	Poor (voltage fluctuations due to wind variations)	Improved (STATCOM compensates for voltage dips and surges)
Reactive Power Support	Insufficient (wind turbines generate or absorb reactive power randomly)	Excellent (STATCOM provides real-time reactive power support)
Fault Ride-Through (FRT) Capability	Weak (wind turbine may disconnect during faults)	Strong (helps wind turbine stay connected during faults)
Power Factor	Low (depends on wind turbine's operating conditions)	High (STATCOM maintains unity power factor)
Harmonic Distortion	High (wind inverters introduce harmonics into the grid)	Reduced (STATCOM filters and compensates for harmonics)
Grid Compliance	May not meet grid code requirements (especially for weak grids)	Meets grid code requirements (ensures stable grid operation)
Voltage Regulation Time	Slow response to wind speed variations	Fast response to wind disturbances
Transmission Efficiency	Lower (more reactive power losses in the network)	Higher (reactive power compensation reduces losses)

9 CONCLUSION

The integration of wind turbines into the grid offers opportunities but also presents stability challenges. Effective technological, economic, and regulatory frameworks are essential for wind energy to contribute significantly to decarbonization. This study examined grid integration involving a conventional power plant, wind farm, load, and STATCOM for voltage stabilization. Simulation results demonstrated that without STATCOM, voltage instability, poor reactive power control, and grid compliance issues occur. However, integrating STATCOM improves voltage stability, power factor, fault ride-through, and grid reliability. STATCOM proves particularly valuable for weak networks, offshore wind farms, and large wind farms connected to the grid.

Acknowledgement

The authors extend their appreciation to the Deanship of Scientific Research at Northern Border University, Arar, KSA, for funding this research work through the project number NBU-FFR-2025-2484-13.

10 REFERENCES

[1] Wang, S., Zheng, C., Ma, T., Wang, T., Gao, S., Dai, Q., & Chu, F. (2024). Tooth backlash inspired comb-shaped single-electrode triboelectric nanogenerator for self-powered condition monitoring of gear transmission. *Nano Energy*, *123*, 109429. https://doi.org/10.1016/j.nanoen.2024.109429

[2] Zhi, S., Wu, H., Shen, H., Wang, T., & Fu, H. (2024). Entropy-Aided Meshing-Order Modulation Analysis for Wind Turbine Planetary Gear Weak Fault Detection under Variable Rotational Speed. *Entropy*, *26*(5), 409. https://doi.org/10.3390/e26050409

[3] Zhang, J., Li, H., Kong, X., Zhou, J., Shi, G., Zang, J., & Wang, J. (2024). A Novel Multiple-Medium-AC-Port Power Electronic Transformer. *IEEE Transactions on Industrial Electronics*, *71*(7), 6568-6578. https://doi.org/10.1109/TIE.2023.3301550

[4] Zhang, J., Feng, X., Zhou, J., Zang, J., Wang, J., Shi, G., & Li, Y. (2023). Series-Shunt Multiport Soft Normally Open Points. *IEEE Transactions on Industrial Electronics*, *70*(11), 10811-10821. https://doi.org/10.1109/TIE.2022.3229375

[5] Zhao, D., Shao, D., & Cui, L. (2024). CTNet: A data-driven time-frequency technique for wind turbines fault diagnosis under time-varying speeds. *ISA Transactions*, *154*, 335-351. https://doi.org/10.1016/j.isatra.2024.08.029

[6] Li, M., Wang, T., Chu, F., Han, Q., Qin, Z., & Zuo, M. J. (2021). Scaling-Basis Chirplet Transform. *IEEE Transactions on Industrial Electronics*, *68*(9), 8777-8788. https://doi.org/10.1109/TIE.2020.3013537

[7] Li, S., Zhou, J., Zhou, F., Niu, F., & Deng, W. (2025). A Reduced Current Ripple Overmodulation Strategy for Indirect Matrix Converter. *IEEE Transactions on Industrial Electronics*, *72*(4), 3768-3777. https://doi.org/10.1109/TIE.2024.3453934

[8] Wu, T., Yang, H., Wang, P., Zhang, C., & Zhang, M. (2024). Data-Driven Fatigue Reliability Evaluation of Offshore Wind Turbines under Floating Ice Loading. *Journal of Structural Engineering*, *150*(12), 5024004. https://doi.org/10.1061/JSENDH.STENG-13476

[9] Zhang, H., Chen, Z., Yu, C., Yue, D., Xie, X., & Hancke, G. P. (2024). Event-Trigger-Based Resilient Distributed Energy Management Against FDI and DoS Attack of Cyber–Physical System of Smart Grid. *IEEE Transactions on Systems, Man, and Cybernetics: Systems*, *54*(5), 3220-3230. https://doi.org/10.1109/TSMC.2024.3357497

[10] Zhang, H., Yue, D., Dou, C., & Hancke, G. P. (2023). PBI Based Multi-Objective Optimization via Deep Reinforcement Elite Learning Strategy for Micro-Grid Dispatch With Frequency Dynamics. *IEEE Transactions on Power Systems*, *38*(1), 488-498. https://doi.org/10.1109/TPWRS.2022.3155750

[11] Wang, X., Guo, Q., Tu, C., Che, L., Xu, Z., Xiao, F., & Chen, L. (2025). A Comprehensive Control Strategy for F-SOP Considering Three-Phase Imbalance and Economic Operation in ISLDN. *IEEE Transactions on Sustainable Energy*, *16*(1), 149-159. https://doi.org/10.1109/TSTE.2024.3444794

[12] Li, Y., Qian, K., Wang, Z., & Xu, A. (2023). The evolution of China's wind power industry innovation network from the perspective of multidimensional proximity. *Technology Analysis & Strategic Management*, 1-15. https://doi.org/10.1080/09537325.2024.2405145

[13] Zhang, X., Zhu, Q., Wang, S., Ma, T., Gao, S., Kong, Y., & Chu, F. (2025). Hybrid triboelectric-variable reluctance generator assisted wireless intelligent condition monitoring of aero-engine main bearings. *Nano Energy*, *136*, 110721. https://doi.org/10.1016/j.nanoen.2025.110721

[14] Hu, X., Li, J., Li, F., Wang, J., & Wang, Y. (2025). Priority rule-based heuristics for distributed multi-project scheduling considering global resource failures. *Journal of the Operational Research Society*, 1-20. https://doi.org/10.1080/01605682.2025.2457655

[15] Zhi, S., Su, K., Yu, J., Li, X., & Shen, H. (2025). An unsupervised transfer learning bearing fault diagnosis method based on multi-channel calibrated Transformer with shiftable window. *Structural Health Monitoring*. https://doi.org/10.1177/14759217251324671

[16] Yi, X., Lu, T., Li, Y., Ai, Q., & Hao, R. (2025). Collaborative planning of multi-energy systems integrating complete hydrogen energy chain. *Renewable and Sustainable Energy Reviews*, *210*, 115147. https://doi.org/10.1016/j.rser.2024.115147

[17] Yang, Y., Zhao, Y., Yan, G., Mu, G., & Chen, Z. (2024). Real time aggregation control of P2H loads in a virtual power plant based on a multi-period stackelberg game. *Energy*, *303*, 131484.

https://doi.org/10.1016/j.energy.2024.131484
[18] Rong, Q., Hu, P., Yu, Y., Wang, D., Cao, Y., & Xin, H. (2025). Virtual External Perturbance-Based Impedance Measurement of Grid-Connected Converter. *IEEE Transactions on Industrial Electronics*, *72*(3), 2644-2654. https://doi.org/10.1109/TIE.2024.3436629
[19] Rong, Q., Hu, P., Wang, L., Li, Y., Yu, Y., Wang, D., & Cao, Y. (2024). Asymmetric Sampling Disturbance-Based Universal Impedance Measurement Method for Converters. *IEEE Transactions on Power Electronics*, *39*(12), 15457-15461. https://doi.org/10.1109/TPEL.2024.3451403
[20] Zhang, Z., Bu, Y., Wu, H., Wu, L., & Cui, L. (2023). Parametric study of the effects of clump weights on the performance of a novel wind-wave hybrid system. *Renewable Energy*, *219*(Part 1), 119464. https://doi.org/10.1016/j.renene.2023.119464
[21] Gao, S., Chen, Y., Song, Y., Yu, Z., & Wang, Y. (2024). An Efficient Half-Bridge MMC Model for EMTP-Type Simulation Based on Hybrid Numerical Integration. *IEEE Transactions on Power Systems*, *39*(1), 1162-1177. https://doi.org/10.1109/TPWRS.2023.3262584
[22] Wang, J., Zhang, B., Zhao, Z., Gao, Y., Liu, D., Liu, X., & Wang, J. (2024). Boosting the Charge Density of Triboelectric Nanogenerator by Suppressing Air Breakdown and Dielectric Charge Leakage. *Advanced Energy Materials*, *14*(8), 2303874. https://doi.org/10.1002/aenm.202303874
[23] Hu, Y., Li, X., Gao, Y., Zhao, Z., Liu, X., He, L., & Wang, J. (2024). A Combined Wind Harvesting and Speed Sensing System Based on Constant-Voltage Triboelectric Nanogenerator. *Advanced Energy Materials*, *14*(23), 2400672. https://doi.org/10.1002/aenm.202400672
[24] Zhang, C., Liu, M., Liu, Z., Sabetahd, R., Taghavifar, H.,...Mohammadzadeh, A. (2024). A multiple model type-3 fuzzy control for offshore wind turbines using the Active Rotary Inertia Driver (ARID). *Ocean Engineering*, *313*, 119337. https://doi.org/10.1016/j.oceaneng.2024.119337
[25] Xia, Y., Huang, Y., & Fang, J. (2025). A generalized Nash-in-Nash bargaining solution to allocating energy loss and network usage cost of buildings in peer-to-peer trading market. *Sustainable Energy, Grids and Networks*, *42*, 101628. https://doi.org/10.1016/j.segan.2025.101628
[26] Zhao, H., Zong, Q., Zhou, H., Yao, W., Sun, K., Zhou, Y., & Wen, J. (2025). Frequency-Voltage Active Support Strategy for Hybrid Wind Farms Based on Grid-Following and Grid-Forming Hierarchical Subgroup Control. *CSEE Journal of Power and Energy Systems*, *11*(1), 65-77. https://doi.org/10.17775/CSEEJPES.2024.02340
[27] Shen, Y., Lu, Q., & Li, Y. (2023). Design Criterion and Analysis of Hybrid-Excited Vernier Reluctance Linear Machine With Slot Halbach PM Arrays. *IEEE Transactions on Industrial Electronics*, *70*(5), 5074-5084. https://doi.org/10.1109/TIE.2022.3183278
[28] Shen, Y., Li, Z., Zeng, Z., Lu, Q., & Lee, C. H. T. (2024). Quantitative Analysis of Asymmetric Flux Reversal Permanent Magnet Linear Machine for Long Excursion Application. *IEEE Transactions on Industrial Electronics*, *71*(10), 12781-12792. https://doi.org/10.1109/TIE.2023.3344854
[29] Zhang, T., Zhao, W., He, Q., & Xu, J. (2025). Optimization of Microgrid Dispatching by Integrating Photovoltaic Power Generation Forecast. *Sustainability*, *17*(2), 648. https://doi.org/10.3390/su17020648
[30] Yang, M., Han, C., Zhang, W., Fang, G., & Jia, Y. (2025). A short-term power prediction method based on numerical weather prediction correction and the fusion of adaptive spatiotemporal graph feature information for wind farm cluster. *Expert Systems with Applications*, *274*, 126979. https://doi.org/10.1016/j.eswa.2025.126979
[31] Yang, M., Xu, C., Bai, Y., Ma, M., & Su, X. (2025). Investigating Black-Box Model for Wind Power Forecasting Using Local Interpretable Model-Agnostic Explanations Algorithm. *CSEE Journal of Power and Energy Systems*, *11*(1), 227-242. https://doi.org/10.17775/CSEEJPES.2021.07470

Abbreviations

ρ	air density	*kg/ m3*
V	Wind speed	m/s
λ	specific speed	-
β	pitch angle	deg
Cp	power coefficient	-
Pt	Power turbine	W
S	Swept area of the blades	m2
Ωr	mechanical speed	rad/s
ωr	Rotor pulsation	rad/s
p	pole pairs	-

Contact information:

Bouaziz LAILA
University of Gabes,
National Engineering School,
Avenue Omar Khattab Gabes 6029, Tunisia
E-mail: bouazizlaila9@gmail.com

Dhaoui MEHDI
University of Gabes,
National Engineering School,
Avenue Omar Khattab Gabes 6029, Tunisia
E-mail: dhaouim@yahoo.fr

Ben Hamed MOUNA
University of Gabes,
National Engineering School,
Avenue Omar Khattab Gabes 6029, Tunisia
E-mail: mouna.benhamed@enig.rnu.tn

Aymen FLAH
1. National Engineering School of Gabes,
University of Gabes,
Zrig, Tunisia
2. Centre for Research Impact and Outcome,
Chitkara University Institute of Engineering and Technology,
Punjab, Rajpura, 140401, India
3. Applied Science Research Center,
Applied Science Private University,
Amman, 11931, Jordan
4. Jadara University Research Center,
Jadara University, Jordan
E-mail: aymen.flah@enig.u-gabes.tn

Habib KRAIEM
(Corresponding author)
Center for Scientific Research and Entrepreneurship,
Northern Border University,
Arar 73213, Saudi Arabia
E-mail: alhabeeb.kareem@nbu.edu.sa

Mishari Metab ALMALKI
Department of Electrical Engineering,
Faculty of Engineering,
Al-Baha University, 65779-7738 Alaqiq, Saudi Arabia
E-mail: mmalmalki@bu.edu.sa

Ahmad A. MOUSA
Department of Basic Sciences,
Middle East University,
Amman 11831, Jordan
E-mail : amousa@meu.edu.jo